Supporting Information

Borane-Protected Cyanides as Surrogates of H-Bonded Cyanides in [FeFe]-Hydrogenase Active Site Models

Brian C. Manor, Mark R. Ringenberg, and Thomas B. Rauchfuss*
School of Chemical Sciences, University of Illinois, Urbana, Illinois 61801, United States

Table of Contents

Experimental Procedures

K_2[Fe_2(adt)$(CO)_4(CN)_2$], K_2[3]
A two-necked Schlenk flask was charged with $Fe_2(adt)(CO)_6$ (0.1 g, 0.26 mmol) and KCN (0.050 g, 0.78 mmol) and suspended in MeCN (20 mL). The mixture was refluxed for 6 h and was mointered by IR for completetion. The mixture was filtered through Celite and the filtrate was dried under vacuum. The resulting solid was washed with Et_2O (20 mL) and hexanes (20 mL) and dried under vaccum. Yield 0.090 g (76%). IR (MeCN, cm^{-1}): ν_{CN} = 2078; ν_{CO} = 1969, 1929, 1893.

$(Et_4N)_2$[Fe_2(pdt)$(CO)_4(CNBPh_3)_2$], $(Et_4N)_2$[1$(BPh_3)_2$]
A solution of $(Et_4N)_2$[**1**] (0.50 g, 0.78 mmol) in CH_2Cl_2 (20 mL) was treated with a solution of BPh_3 (0.38 g, 1.6 mmol) in 20 mL CH_2Cl_2 dropwise. The solvent was evaporated to yield a red oil that was extracted into CH_2Cl_2 (10 mL), layered with pentane (30 mL) and cooled at –30°C for two days producing a red oil. The filtrate was decanted off and the oil was triturated with pentane (3 x 10 mL) to produce a red solid. Yield 0.83 g (94%). Anal. Calcd for $C_{61}B_2Fe_2S_2H_{76}O_4N_4$ (found): C, 65.03 (65.38); H, 6.80 (7.01); N, 4.97 (5.04). IR (CH_2Cl_2, cm^{-1}): ν_{CN} = 2137; ν_{CO} = 1984, 1946, 1911. ^{11}B NMR (CD_2Cl_2) δ–4.5. ^{1}H NMR (CD_2Cl_2): δ7.50 (12H, d, *o*-Ar*H*); δ7.13 (12H, t, *m*-Ar*H*); δ7.01 (6H, t, *p*-Ar*H*); δ2.44 (16H, m, $(CH_3CH_2)_4N$), δ1.96 (4H, t, $SCH_2CH_2CH_2S$), δ1.72 (2H, m, $SCH_2CH_2CH_2$), δ0.84 (24H, t, $(CH_3CH_2)_4N$).

$(Et_4N)_2$[Fe_2(adt)$(CO)_4(CNBPh_3)_2$], $(Et_4N)_2$[3$(BPh_3)_2$]
A solution of $(Et_4N)_2$[**3**] (0.050 g, 0.078 mmol) in CH_2Cl_2 (10 mL) was treated with a solution of BPh_3 (0.038 g, 0.16 mmol) in 10 mL CH_2Cl_2 dropwise. The mixture was filtered through celite and the solvent was evaporated to yield a red oi.l The oil was triturated with pentane (3 x 10 mL) to produce a red solid. Yield 0.070 g (80%). Anal. Calcd for $C_{60}B_2Fe_2S_2H_{75}O_4N_5$ (found): C, 63.90 (63.75); H, 6.70 (6.85); N, 6.21 (5.85). IR (CH_2Cl_2, cm^{-1}): ν_{CN} = 2136; ν_{CO} = 1986, 1949, 1914.

Et_4N[Fe_2(μ-H)(pdt)$(CO)_4(CNBPh_3)_2$], Et_4N[H1$(BPh_3)_2$]
A solution of $(Et_4N)_2$[**1**$(BPh_3)_2$] (100 mg, 0.089 mmol) in CH_2Cl_2 (3 mL) was treated with HCl in ether (0.087 mL, 2 M, 0.178 mmol) resulting in the color of the solution lightening and some percipitate forming. The reaction solution was cooled in a –30°C freezer to precipiate Et_4NCl from solution and was then passed through a plug of celite. The solution was dried under vacuum and the resulting oil was triturated with pentane (3x10 mL) and left to dry under vacuum overnight, yielding a red solid. Yield 85 mg (96 %). IR (CH_2Cl_2, cm^{-1}) ν_{CN} = 2180; ν_{CO} = 2064, 2043, 2009. ^{1}H NMR (CD_2Cl_2): δ –13.2 (s Fe-*H*), δ -16.1 (s Fe-*H*), δ -19.2 (s Fe-*H*).

Table S1. pK_a Determination of $(Et_4N)_2$[**1**$(BAr^F{}_3)_2$] with $PhNH_3BAr^{F24}$ in MeCN.

Run	Initial HB	Initial [**1**$(BR_3)_2$]$^{2□}$	Eq [**1**$(BR_3)_2$]$^{2□}$	Eq [H**1**$(BR_3)_2$]$^{□}$	Eq HB	Eq B	pK_a
1	1.07	1	0.40	0.60	0.47	0.60	10.9
2	0.40	1	0.71	0.29	0.11	0.29	10.7
3	1.91	1	0.26	0.74	1.17	0.74	10.9

pK_a^{MeCN} = 10.8±0.2

Table S2. pK_a Determination of $(Et_4N)_2$[**1**$(BAr^{F\#}{}_3)_2$] with $PyHBAr^{F24}$ in MeCN.

Run	Initial HB	Initial [**1**$(BR_3)_2$]$^{2□}$	Eq [**1**$(BR_3)_2$]$^{2□}$	Eq [H**1**$(BR_3)_2$]$^{□}$	Eq HB	Eq B	pK_a
1	1.33	1	0.16	0.84	0.49	0.84	13.5
2	0.66	1	0.42	0.58	0.08	0.58	13.5
3	2.08	1	0.09	0.91	1.17	0.91	13.4

pK_a^{MeCN} = 13.5±0.1

Table S3. Selected Bond Distances of $[\mathbf{1}(BAr^{F}_{3})_2]^{2\square}$ and $[\mathbf{1}]^{2\square}$ [1]

Bond Distances (Å)	$[\mathbf{1}(BAr^{F}_{3})_2]^{2\square}$	$[\mathbf{1}]^{2\square}$
Fe-Fe	2.519(1)	2.517(2)
$Fe\text{-}CN_{avg}$	1.873(6)	1.93(1)
$C{\equiv}N_{avg}$	1.158(8)	1.16(2)
$Fe\text{-}CO_{avg}$	1.761(10)	1.74(2)
$C{\equiv}O_{avg}$	1.156(10)	1.17(3)

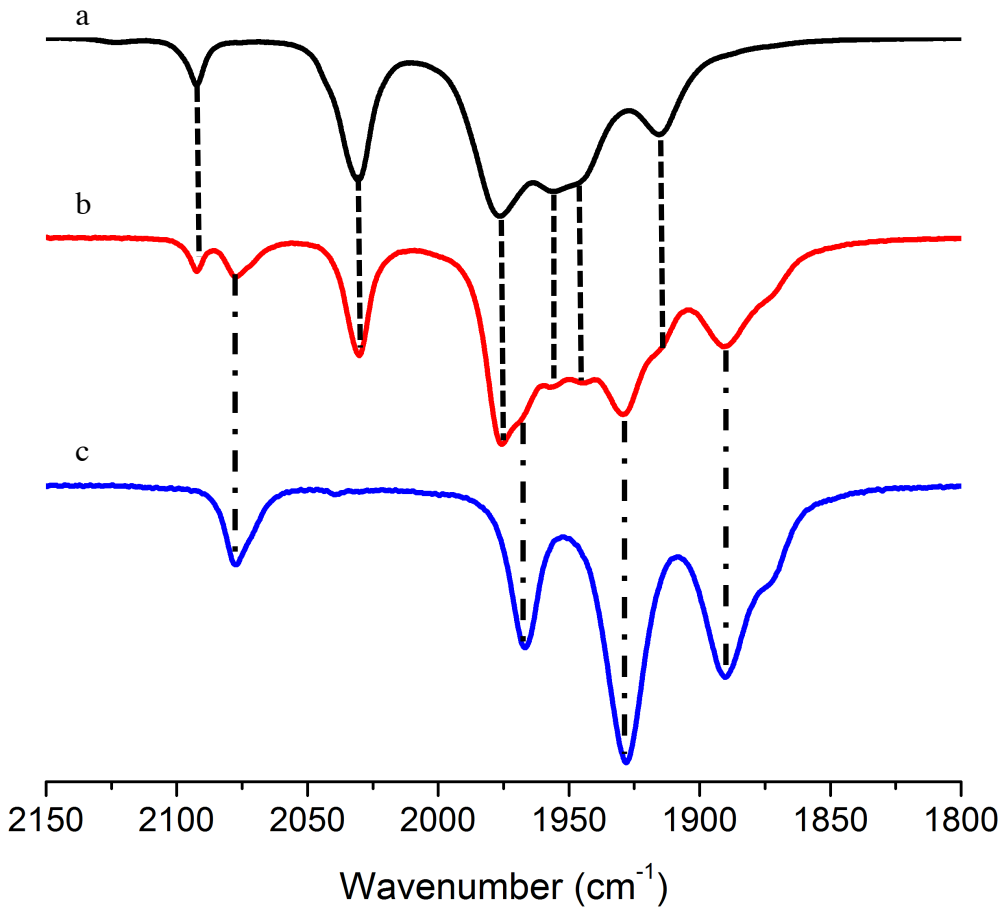

Figure S1. IR spectra in MeCN at 20°C. of a) K[**2**], b) reaction mixture for the synthesis of K_2[**1**] and c) K_2[**1**].

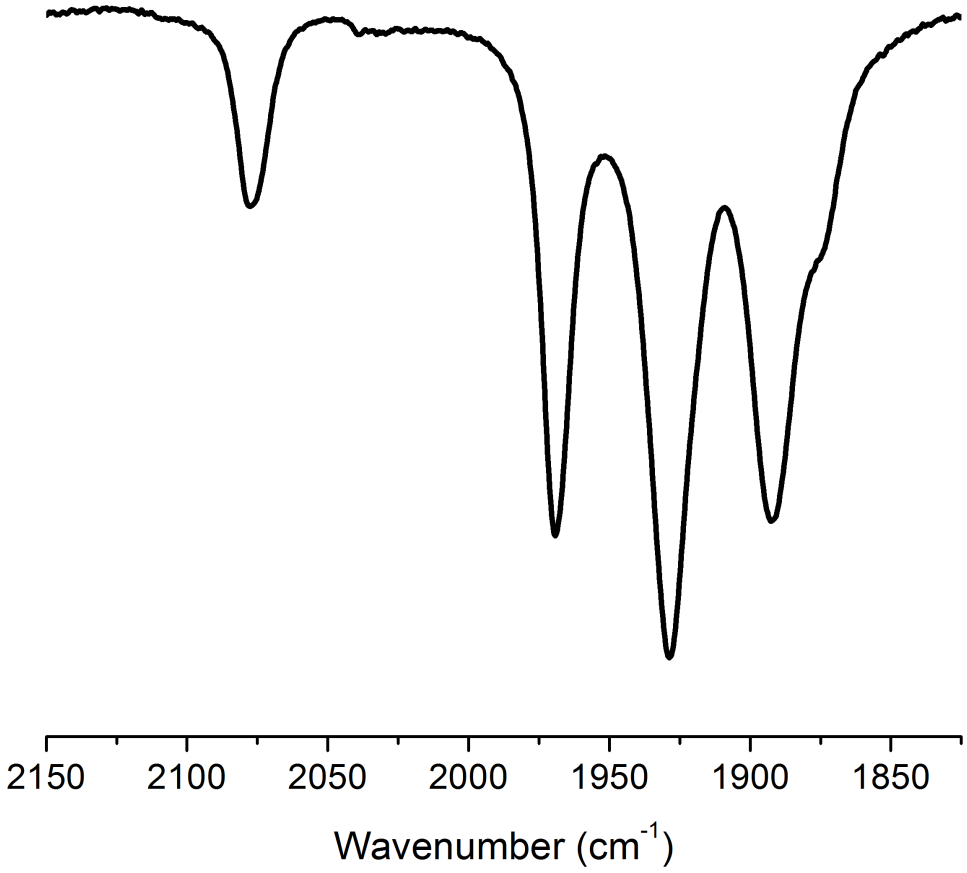

Figure S2. IR spectrum of K_2[**3**] in MeCN at 20°C.

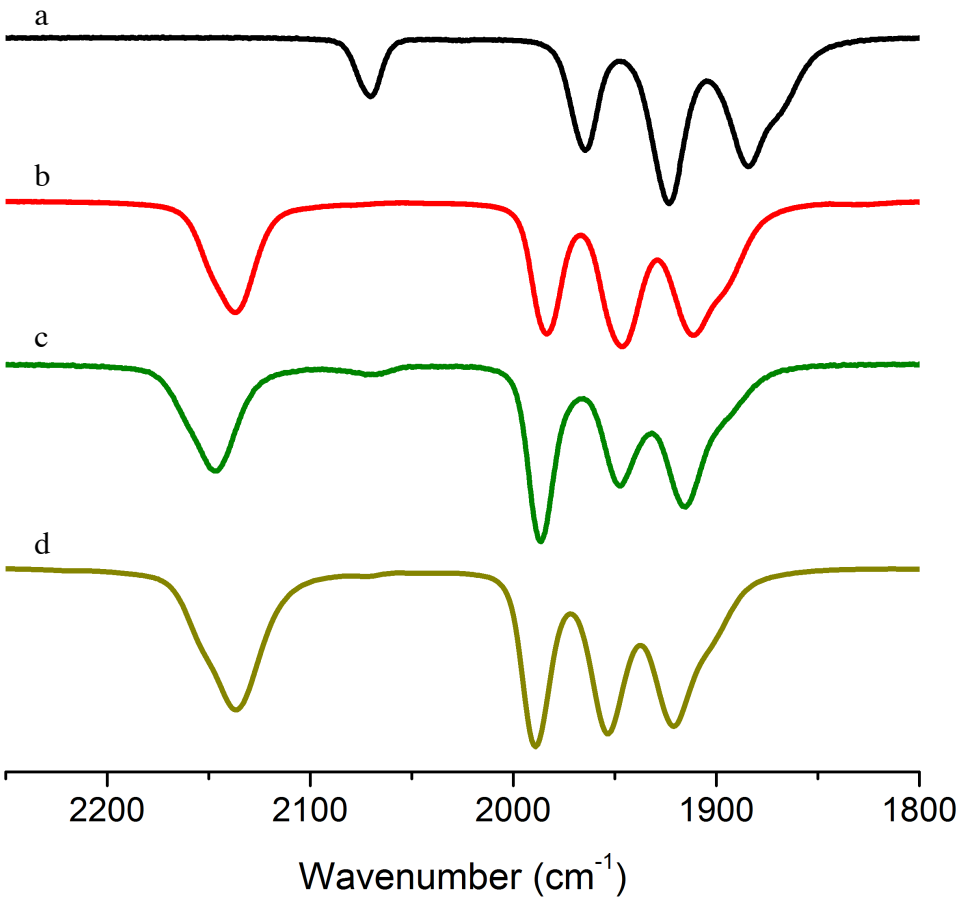

Figure S3. IR spectra of $(Et_4N)_2$[**1**$(BR_3)_2$] complexes in CH_2Cl_2 at 20°C. a) $(Et_4N)_2$[**1**], b) $(Et_4N)_2$[**1**$(BPh_3)_2$], c) $(Et_4N)_2$[**1**$(BAr^{F\#}{}_3)_2$], d) $(Et_4N)_2$[**1**$(BAr^{F}{}_3)_2$].

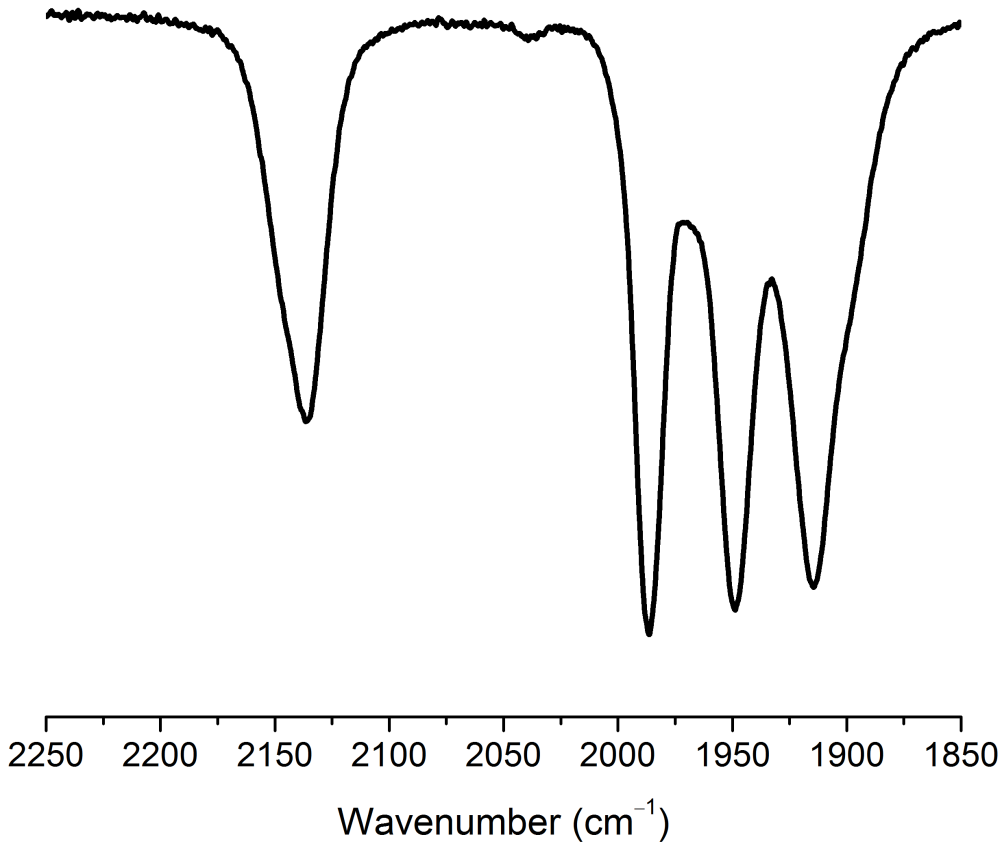

Figure S4. IR spectra of $(Et_4N)_2$[**3**$(BPh_3)_2$] in CH_2Cl_2 at 20°C.

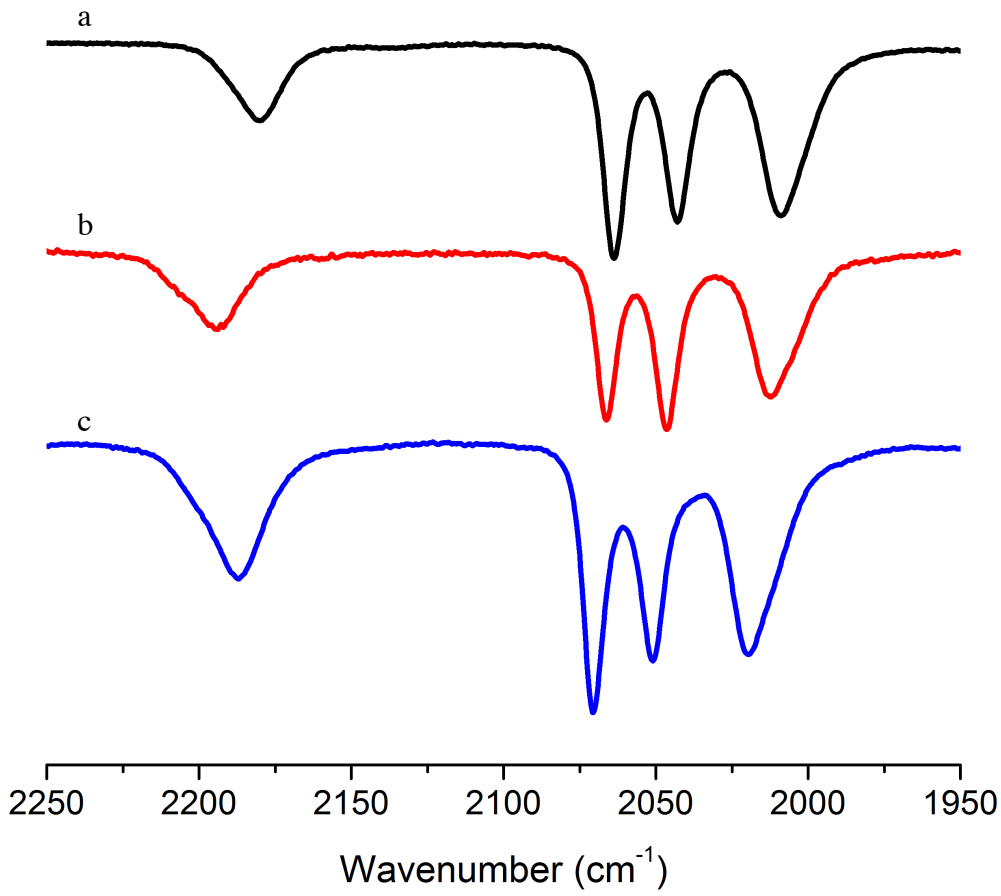

Figure S5. IR spectra of $Et_4N[H\mathbf{1}(BR_3)_2]$ complexes in CH_2Cl_2 at 20°C. a) $Et_4N[H\mathbf{1}(BPh_3)_2]$, b) $Et_4N[H\mathbf{1}(BAr^{F\#}{}_3)_2]$, c) $Et_4N[H\mathbf{1}(BAr^{F}{}_3)_2]$.

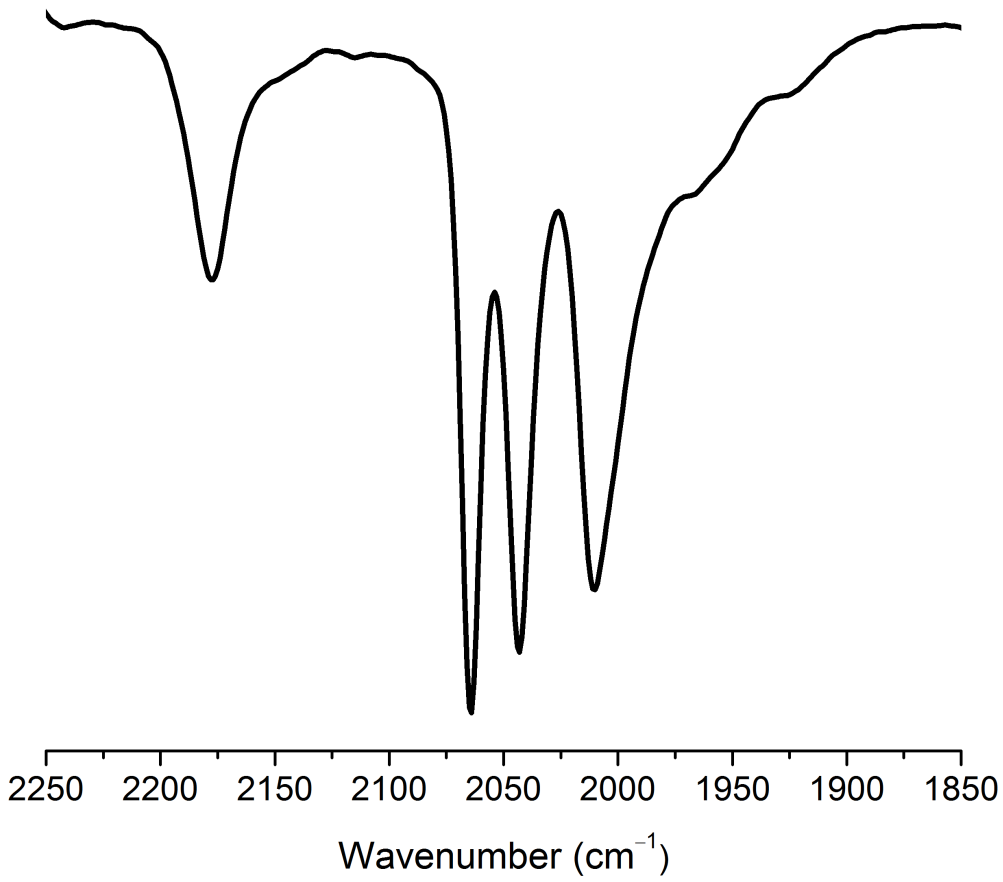

Figure S6. IR spectra of $Et_4N[H\mathbf{3}(BPh_3)_2]$ in CH_2Cl_2 at 20°C.

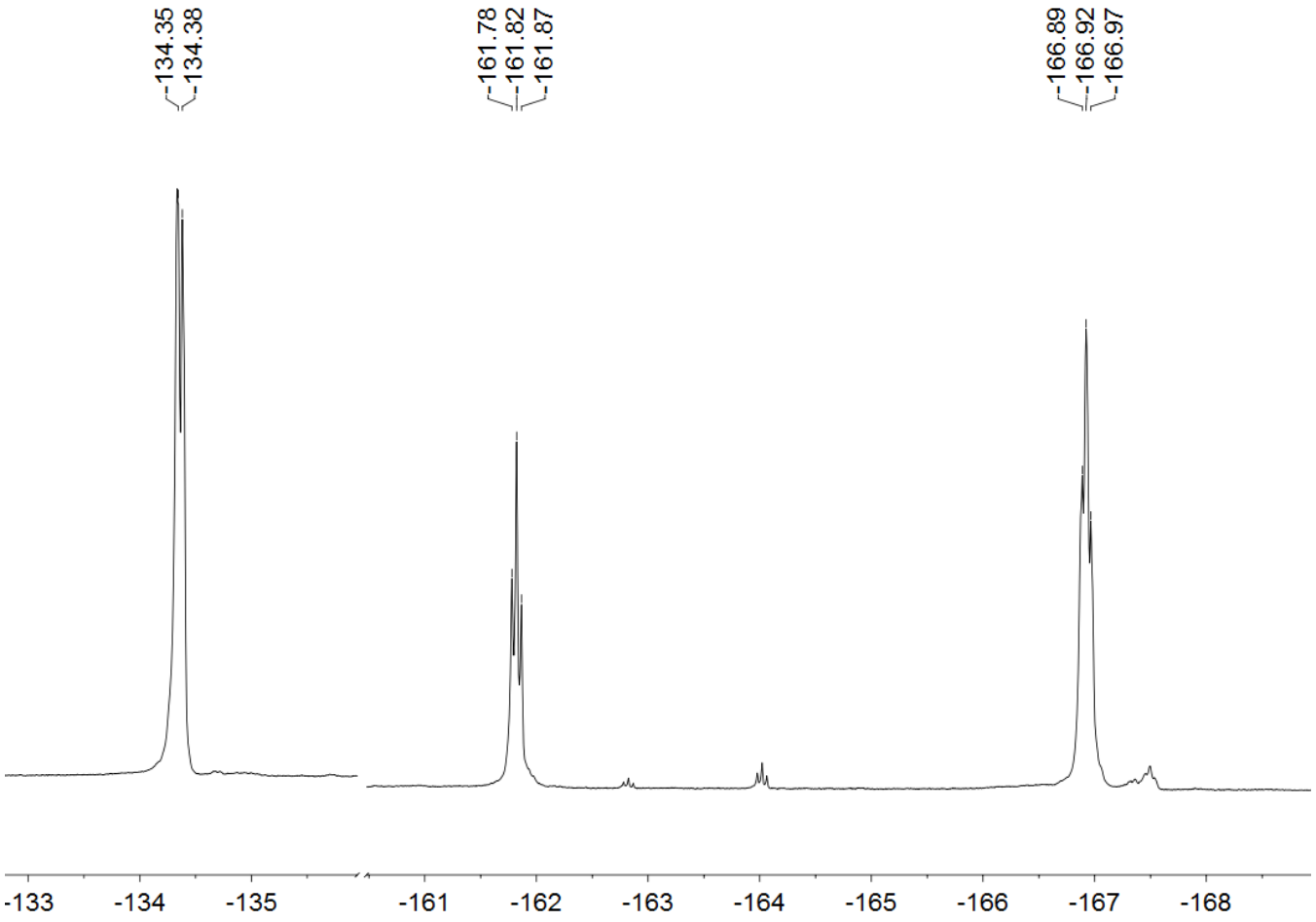

Figure S7. ^{19}F NMR of $(Et_4N)_2[\mathbf{1}(BAr^F{}_3)_2]$ in CD_2Cl_2 at 20°C.

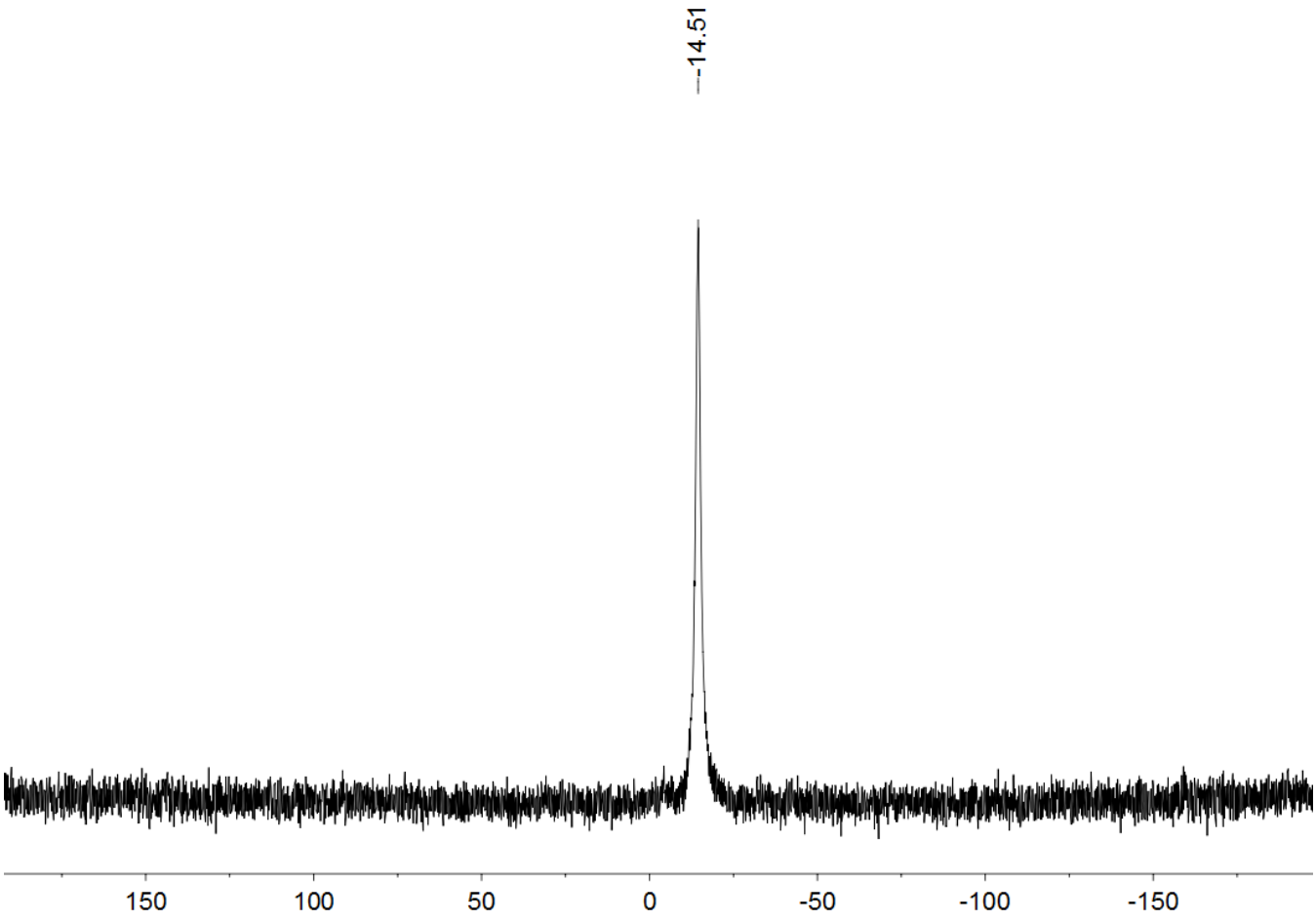

Figure S8. ^{11}B NMR of $(Et_4N)_2[\mathbf{1}(BAr^F{}_3)_2]$ in CD_2Cl_2 at 20°C.

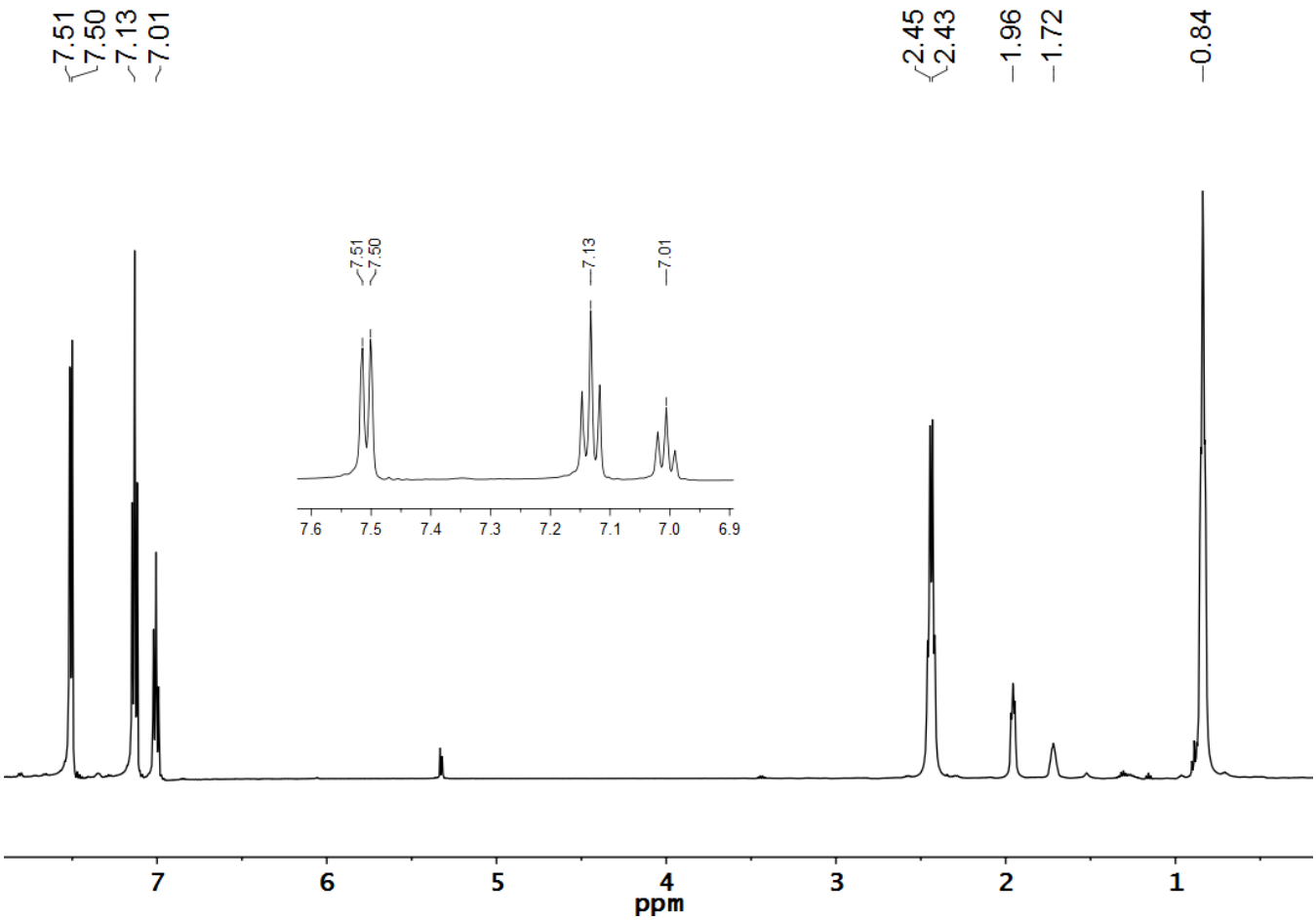

Figure S9. ^{1}H NMR of $(Et_4N)_2[\mathbf{1}(BPh_3)_2]$ in CD_2Cl_2 at 20°C. Inset: ^{1}H NMR signals of aryl region.

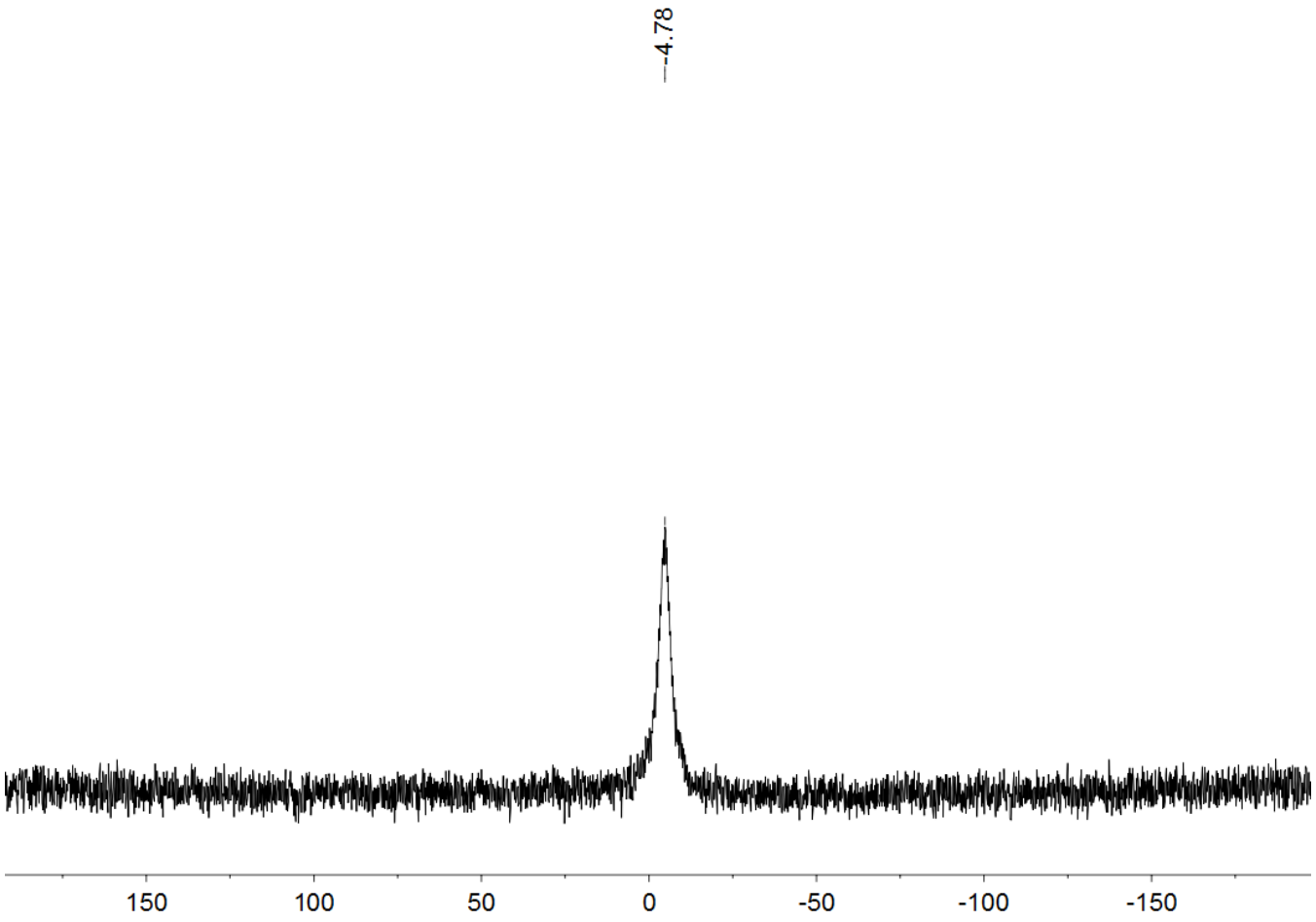

Figure S10. ^{11}B NMR of $(Et_4N)_2[\mathbf{1}(BPh_3)_2]$ in CD_2Cl_2 at 20°C.

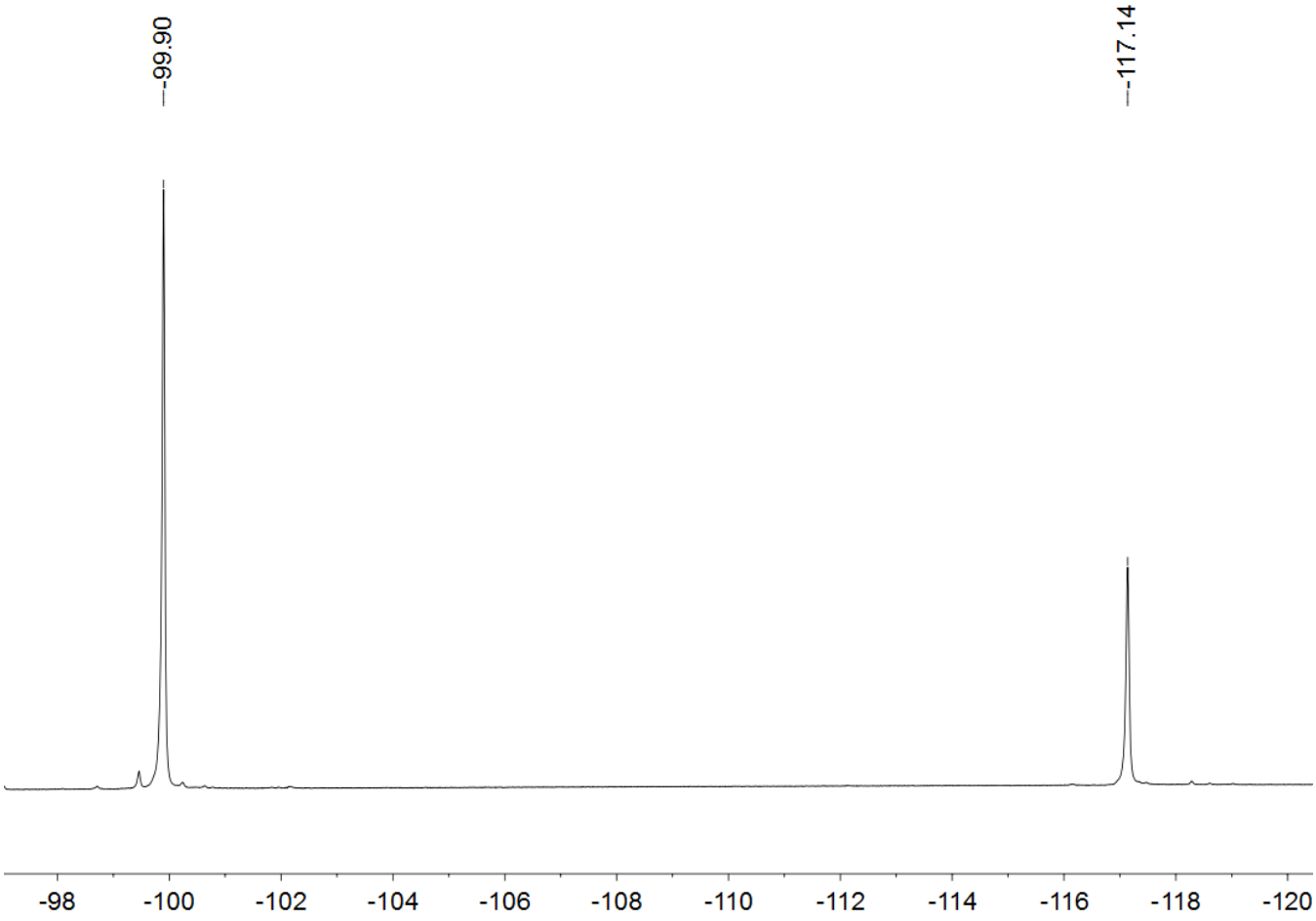

Figure S11. ^{19}F NMR of $(Et_4N)_2[\mathbf{1}(BAr^{F\#}{}_3)_2]$ in CD_2Cl_2 at 20°C.

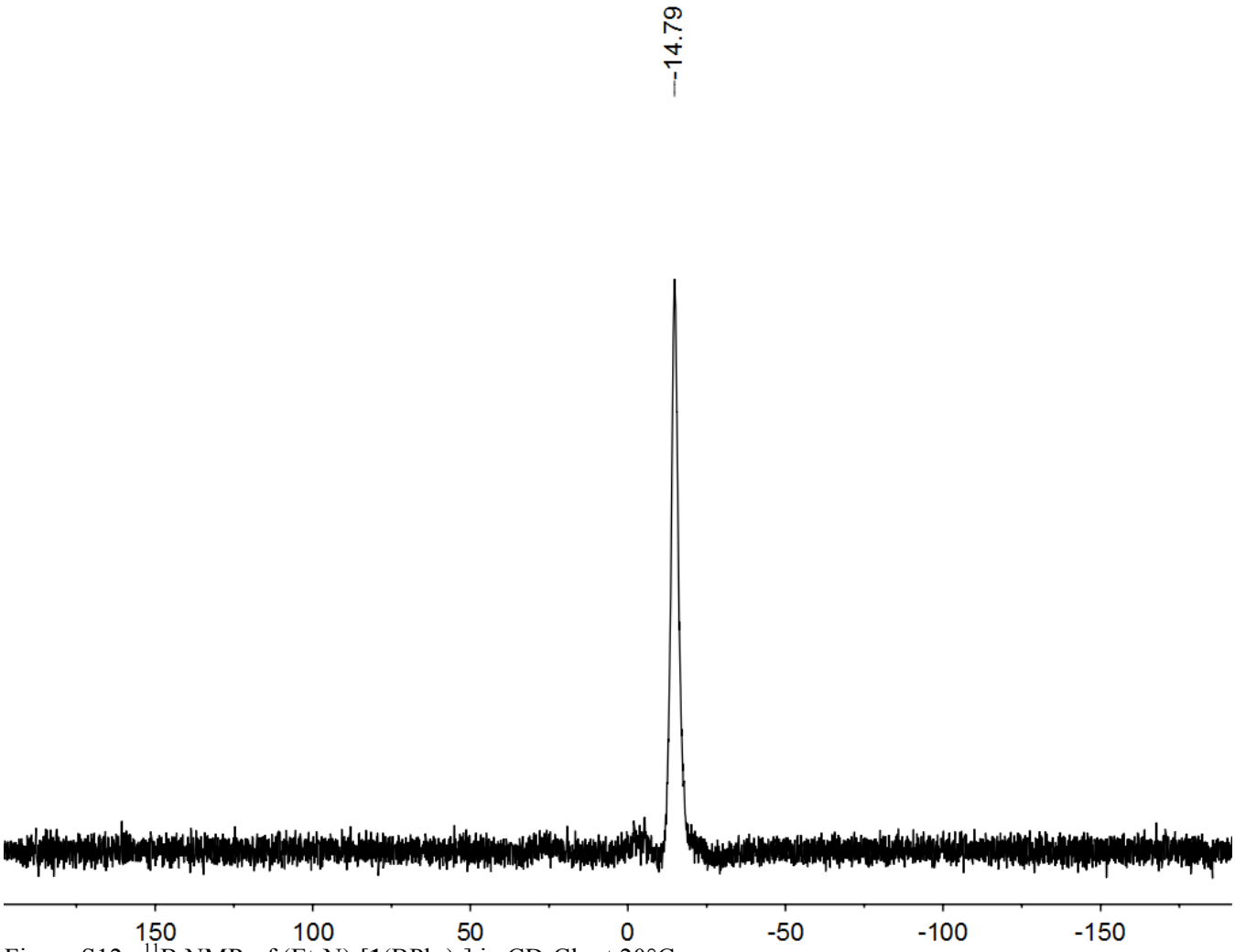

Figure S12. ^{11}B NMR of $(Et_4N)_2[\mathbf{1}(BPh_3)_2]$ in CD_2Cl_2 at 20°C.

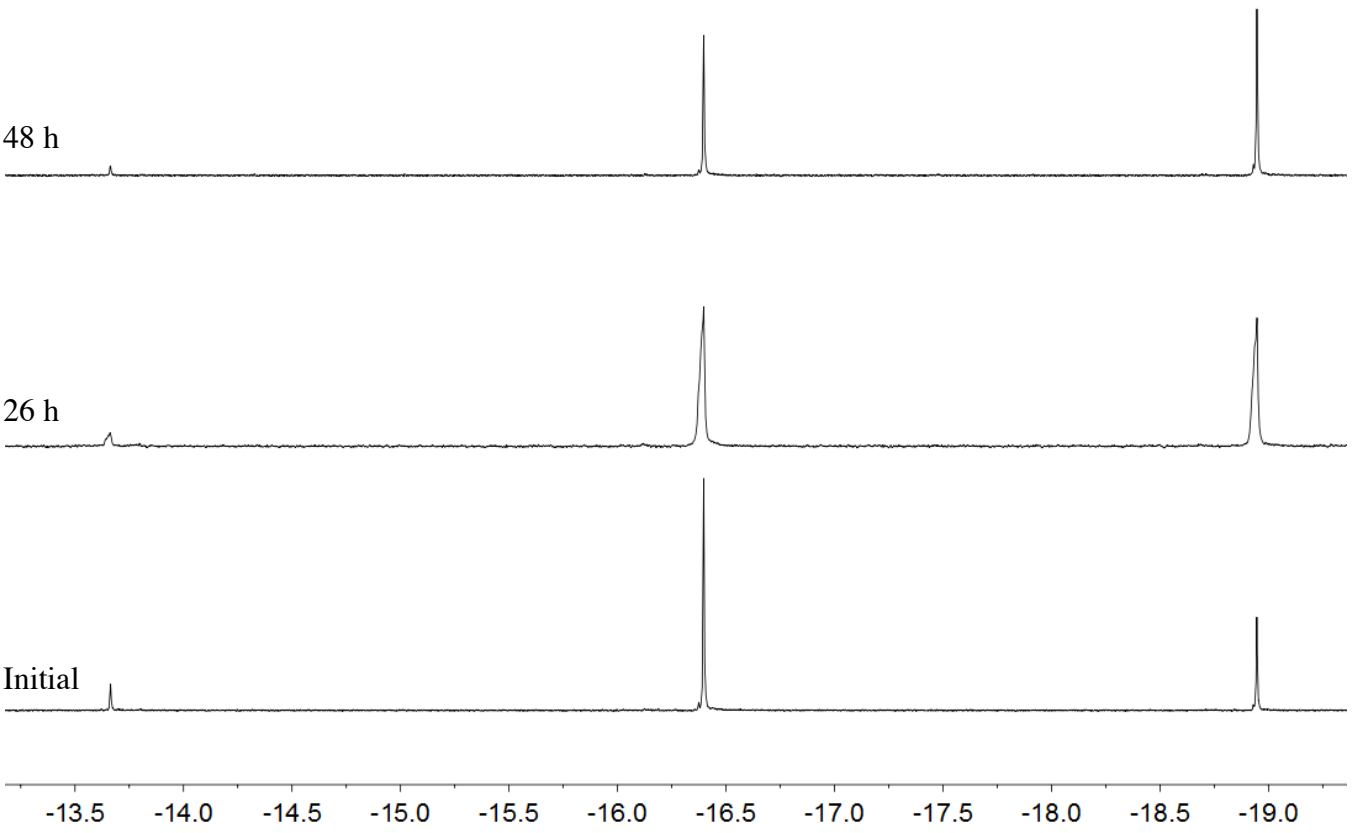

Figure S13. Isomerization of $Et_4N[H\mathbf{1}(BAr^F{}_3)_2]$ in CD_2Cl_2 by ^1H NMR at 20°C.

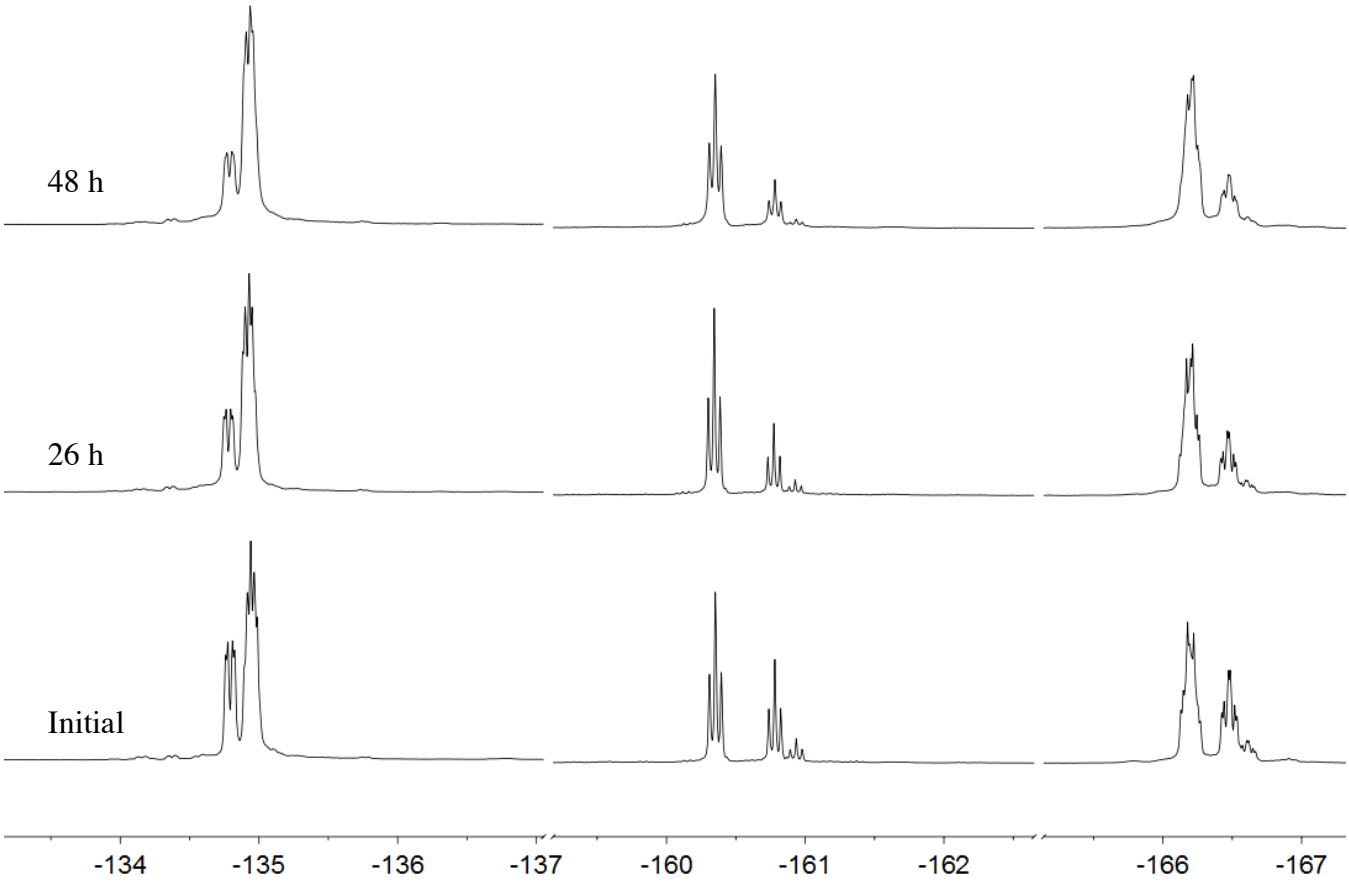

Figure S14. Isomerization of $Et_4N[H\mathbf{1}(BAr^F{}_3)_2]$ in CD_2Cl_2 by ^{19}F NMR at 20°C.

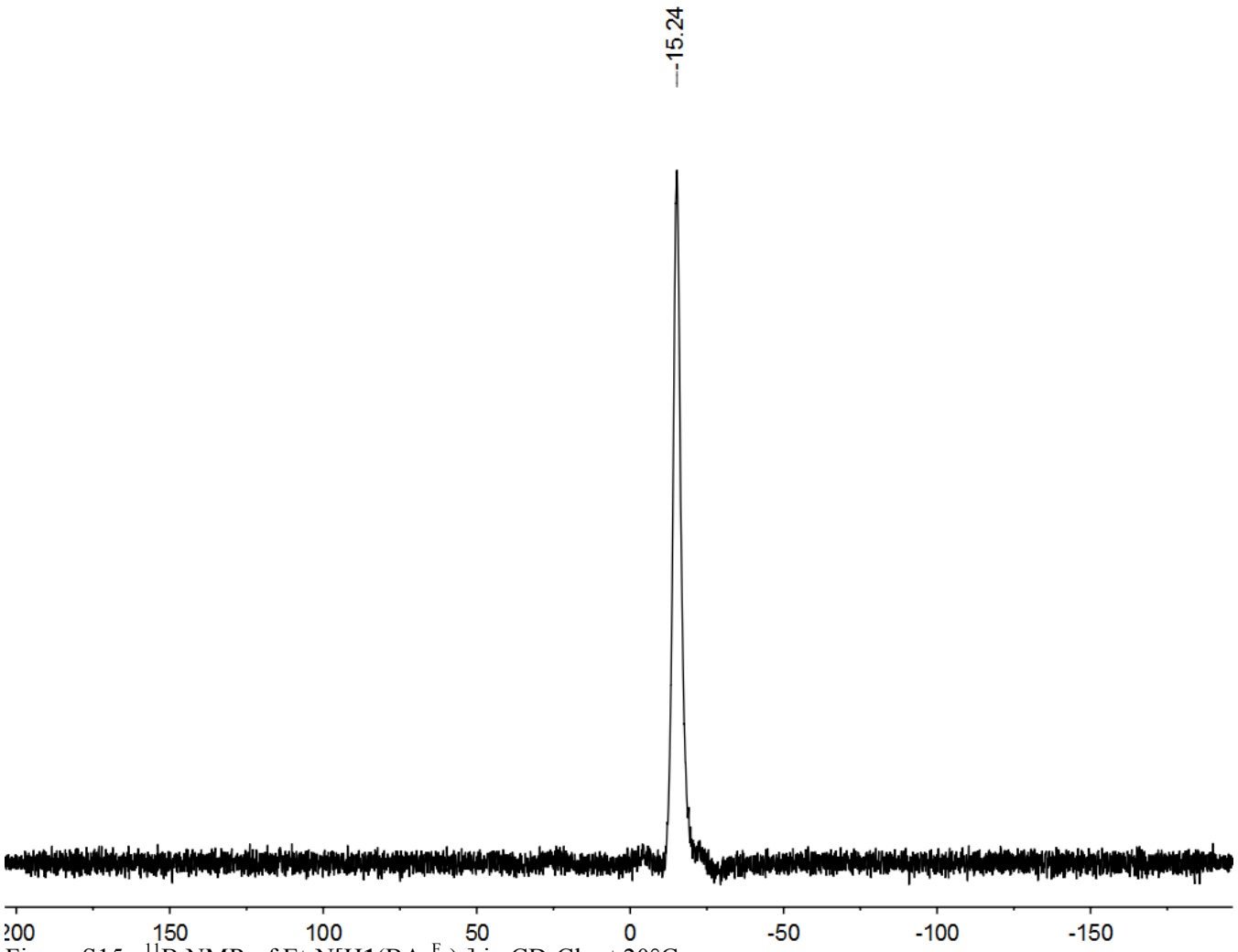

Figure S15. ^{11}B NMR of $Et_4N[H\mathbf{1}(BAr^F{}_3)_2]$ in CD_2Cl_2 at 20°C.

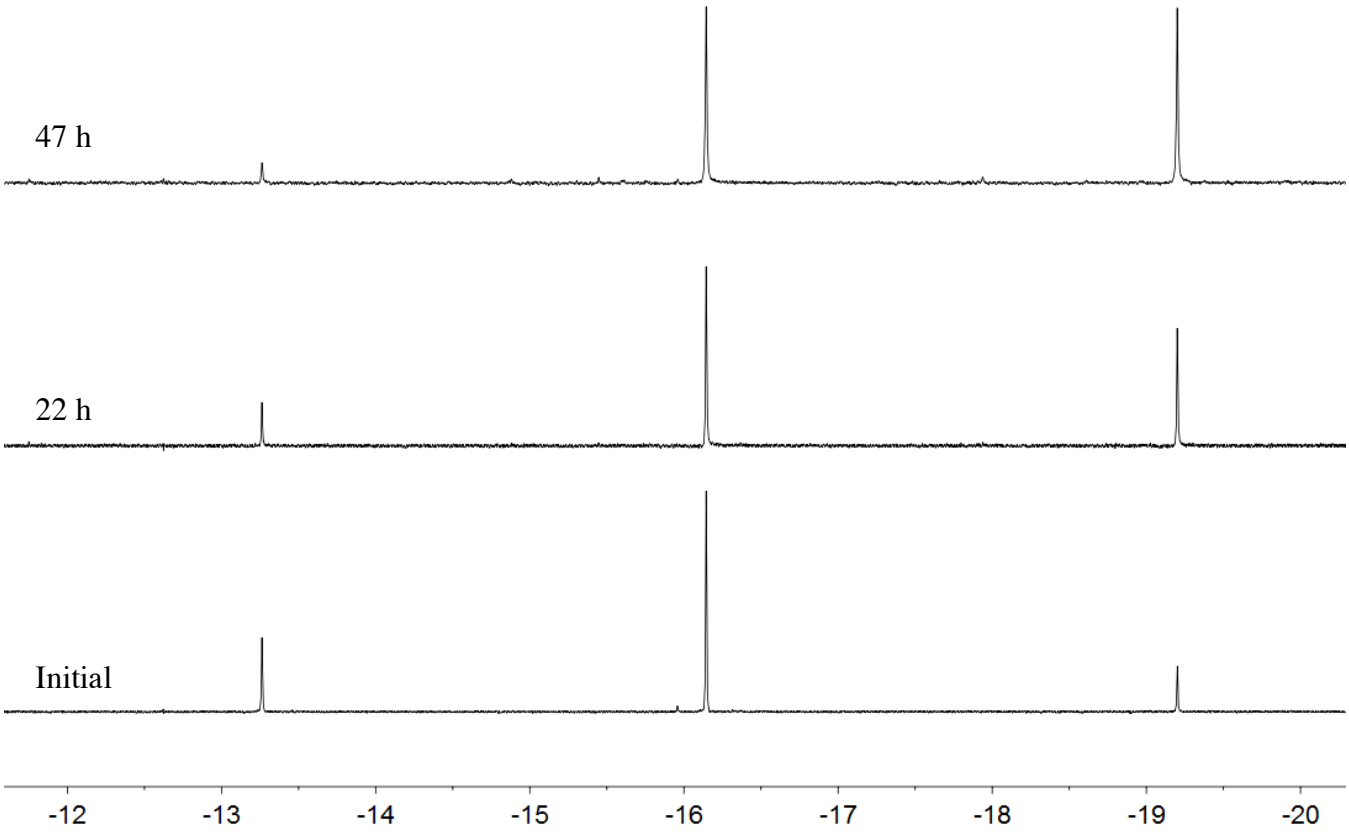

Figure S16. Isomerization of the hydride signals of $Et_4N[H\mathbf{1}(BAr^F{}_3)_2]$ in CD_2Cl_2 by ^1H NMR at 20°C.

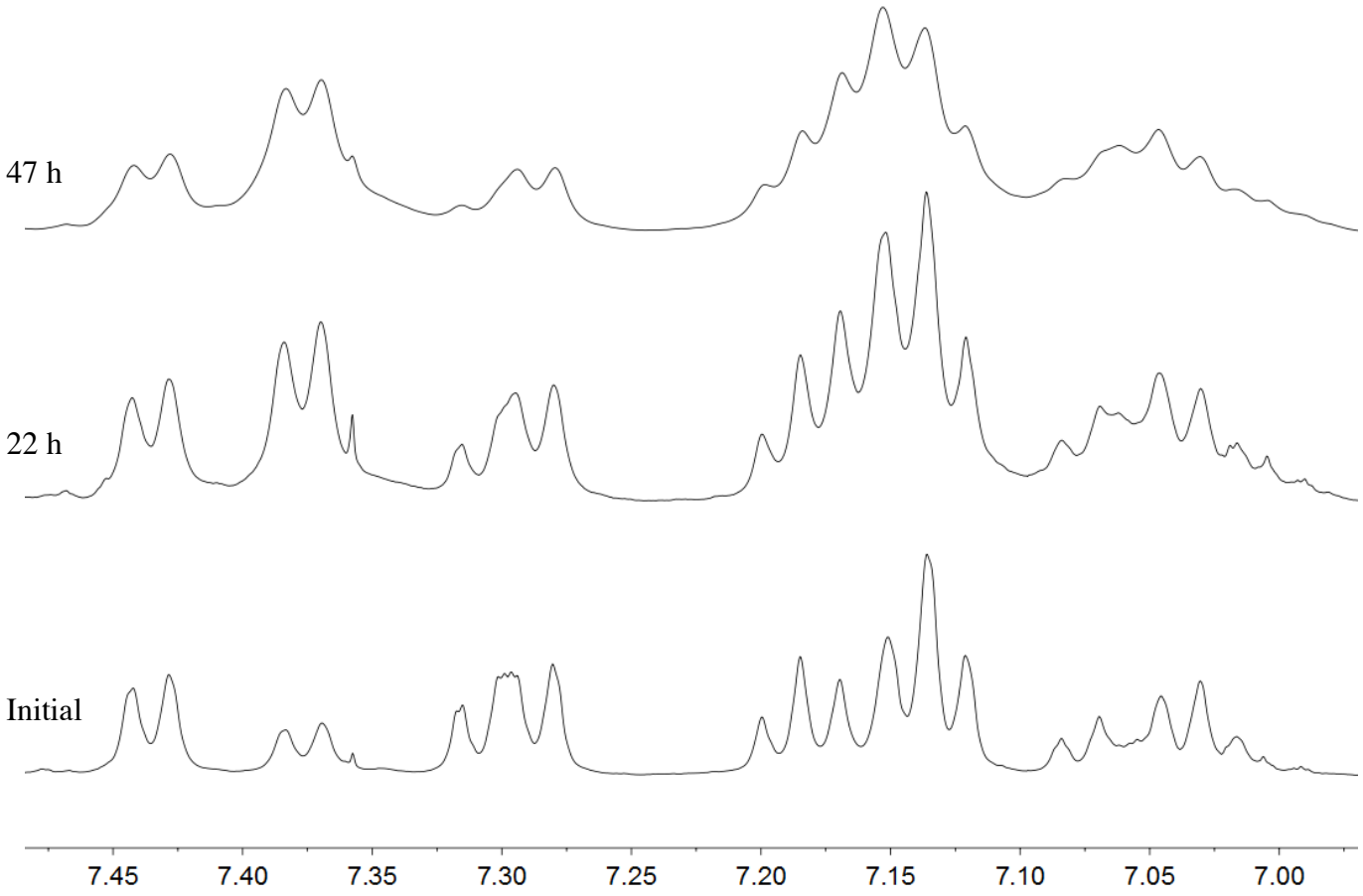

Figure S17. Isomerization of the BPh_3 signals of $Et_4N[H\mathbf{1}(BAr^F{}_3)_2]$ in CD_2Cl_2 by ^1H NMR at 20°C.

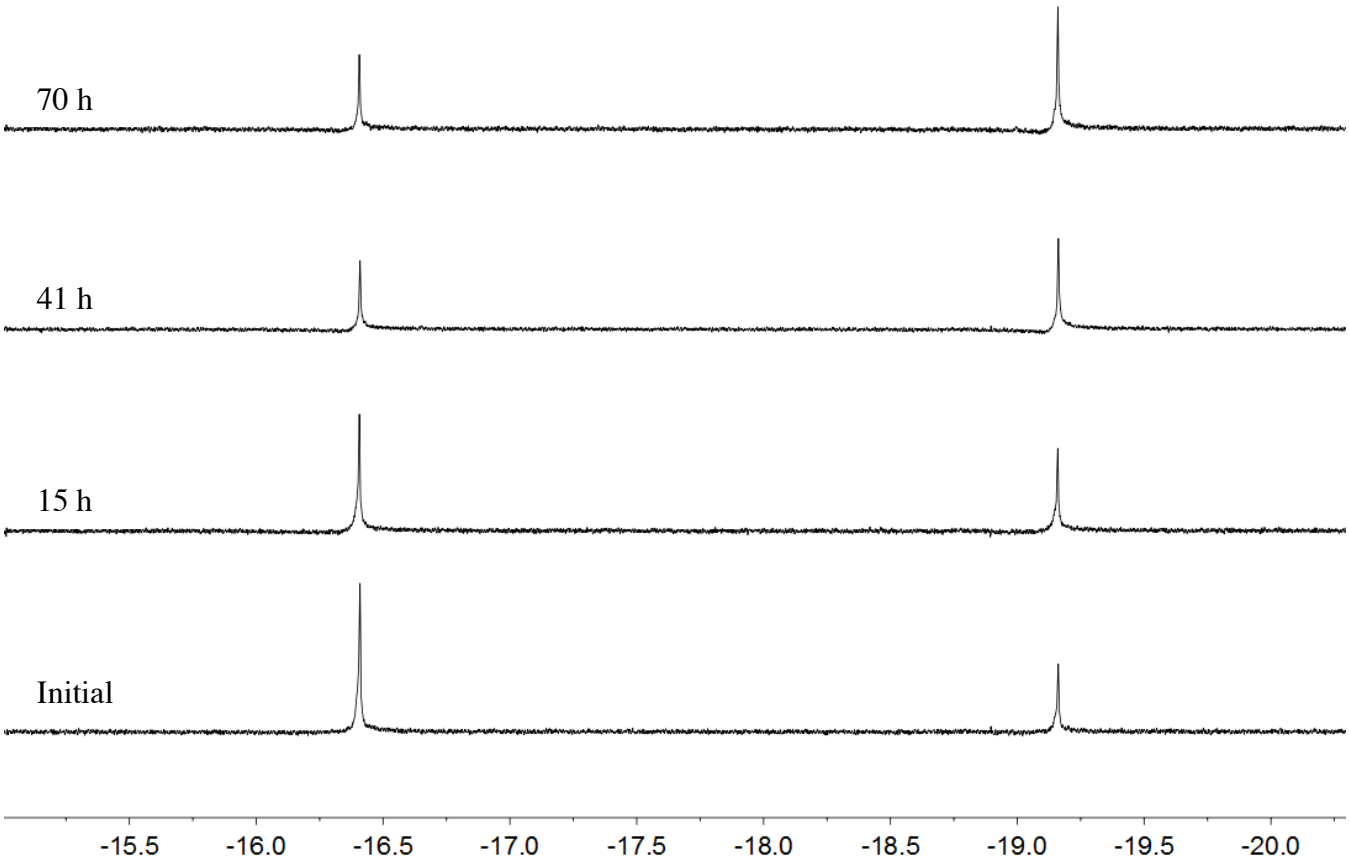

Figure S18. Isomerization of $Et_4N[H\mathbf{1}(BAr^{F\#}{}_3)_2]$ in CD_2Cl_2 monitered by ^1H NMR at 20°C.

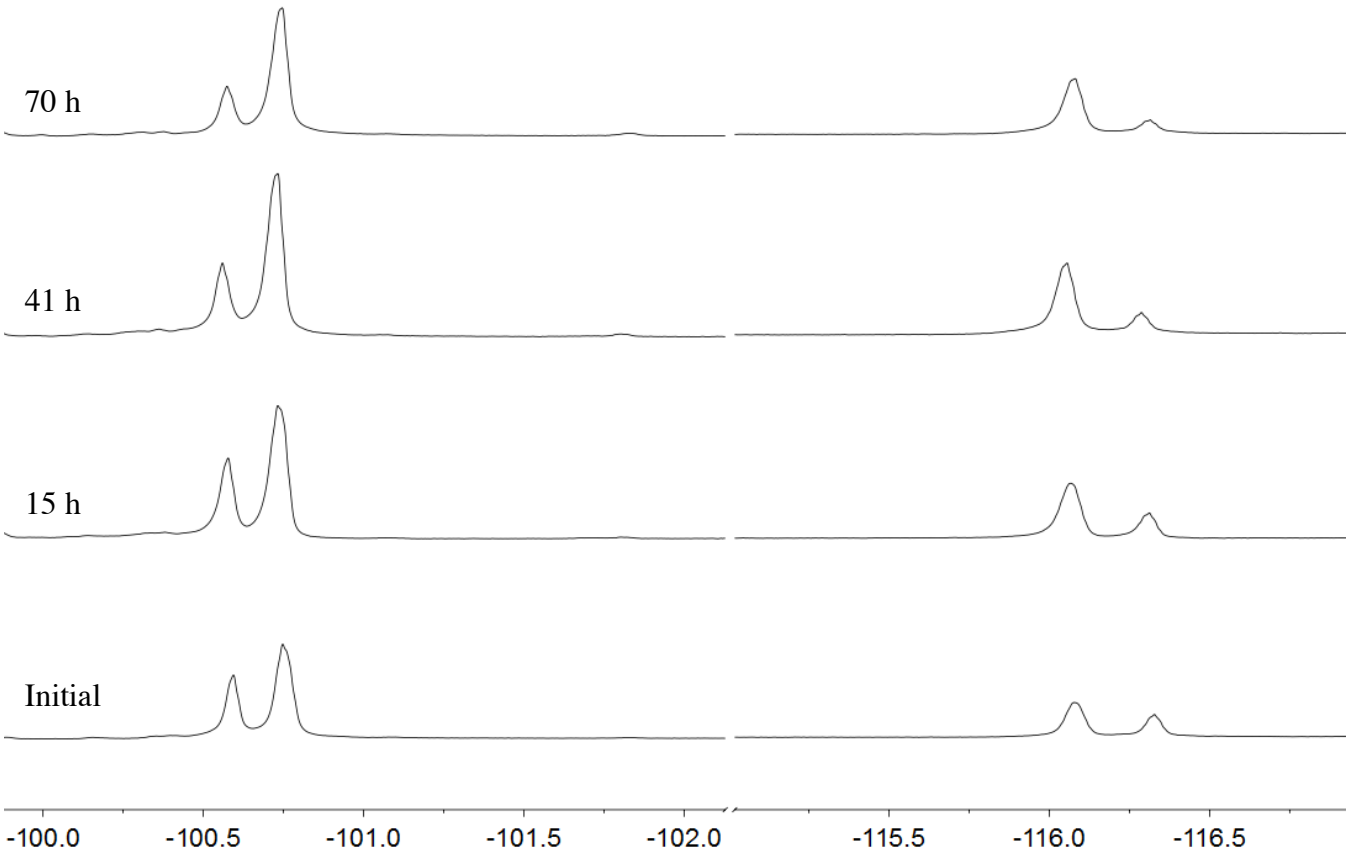

Figure S19. Isomerization of $Et_4N[H\mathbf{1}(BAr^{F\#}{}_3)_2]$ in CD_2Cl_2 monitered by ^{19}F NMR at 20°C.

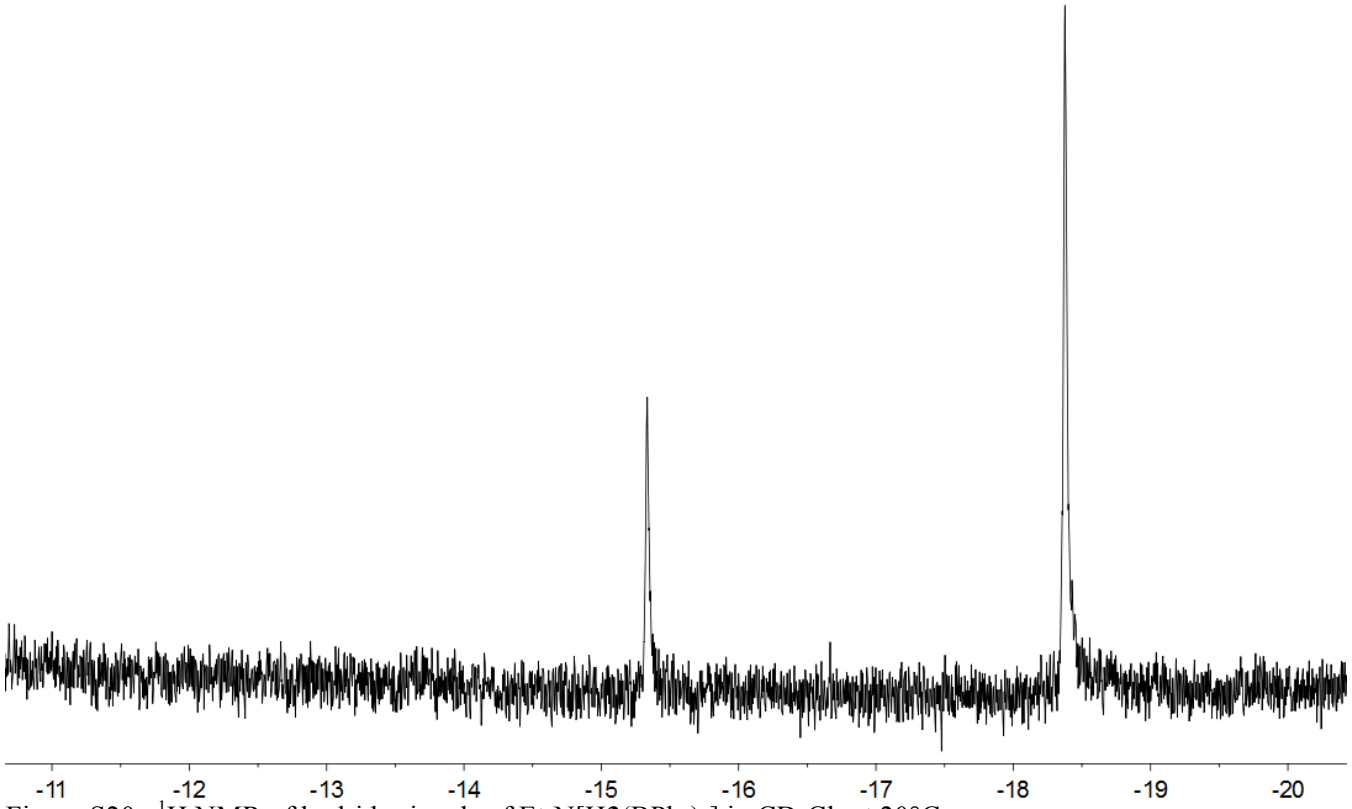

Figure S20. ^{1}H NMR of hydride signals of $Et_4N[H\mathbf{3}(BPh_3)_2]$ in CD_2Cl_2 at 20°C.

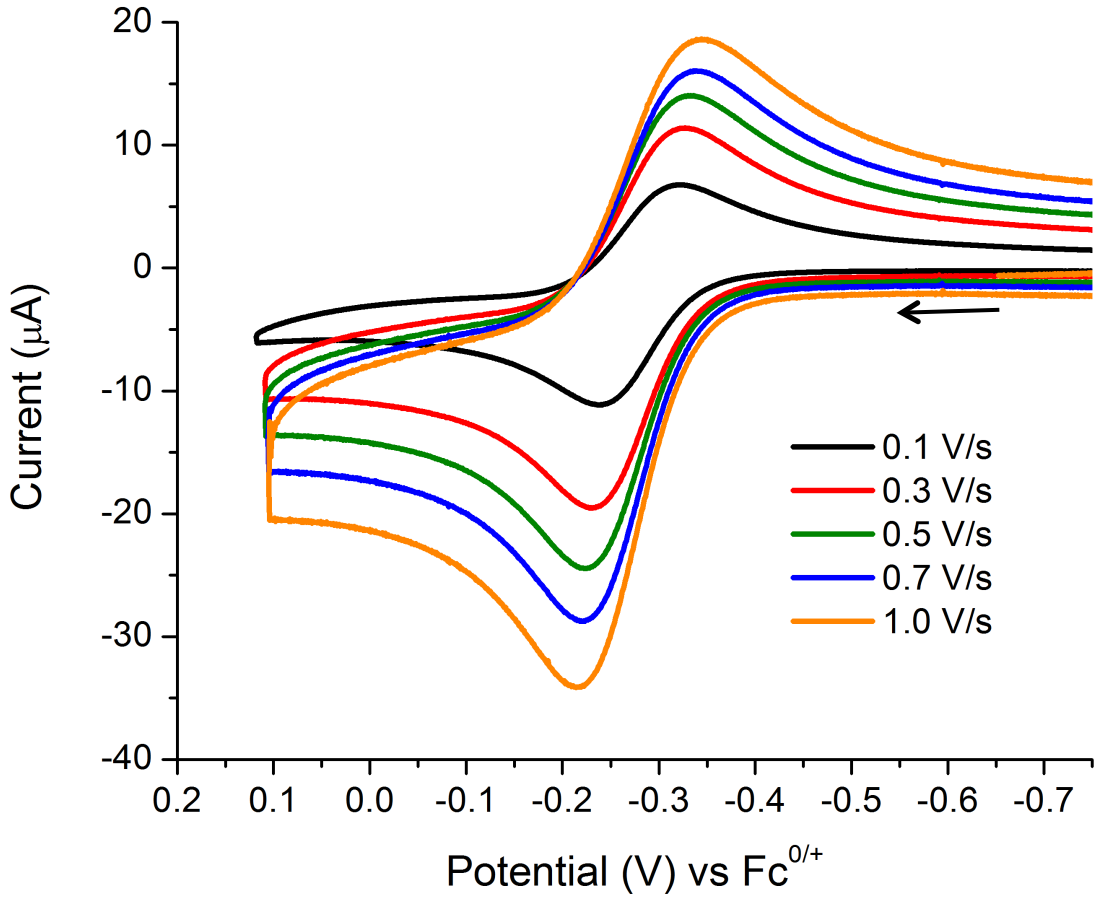

Figure S21. Oxidation of $(Et_4N)_2[\mathbf{1}(BAr^F{}_3)_2]$ in CH_2Cl_2 by Cyclic Voltamogramm.

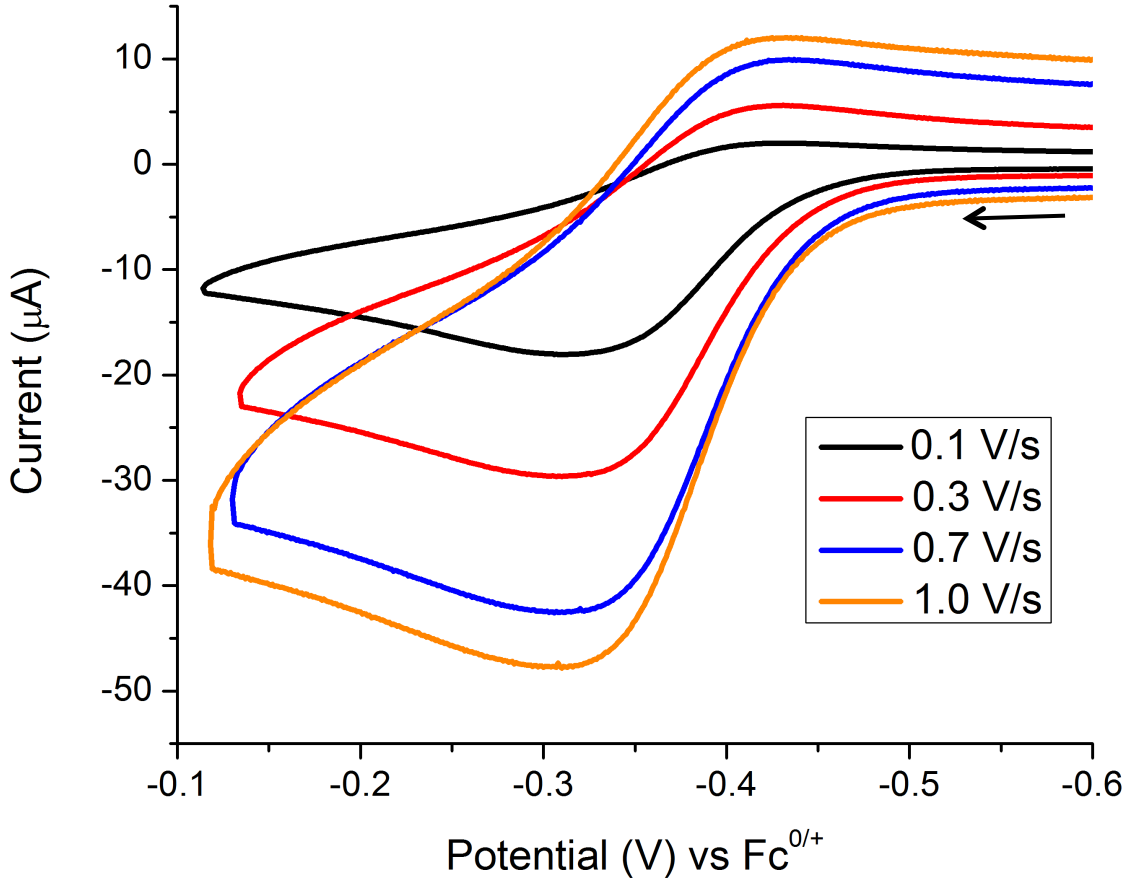

Figure S22. Oxidation of $(Et_4N)_2$[**1**$(BPh_3)_2$] in CH_2Cl_2 by Cyclic Voltamogramm.

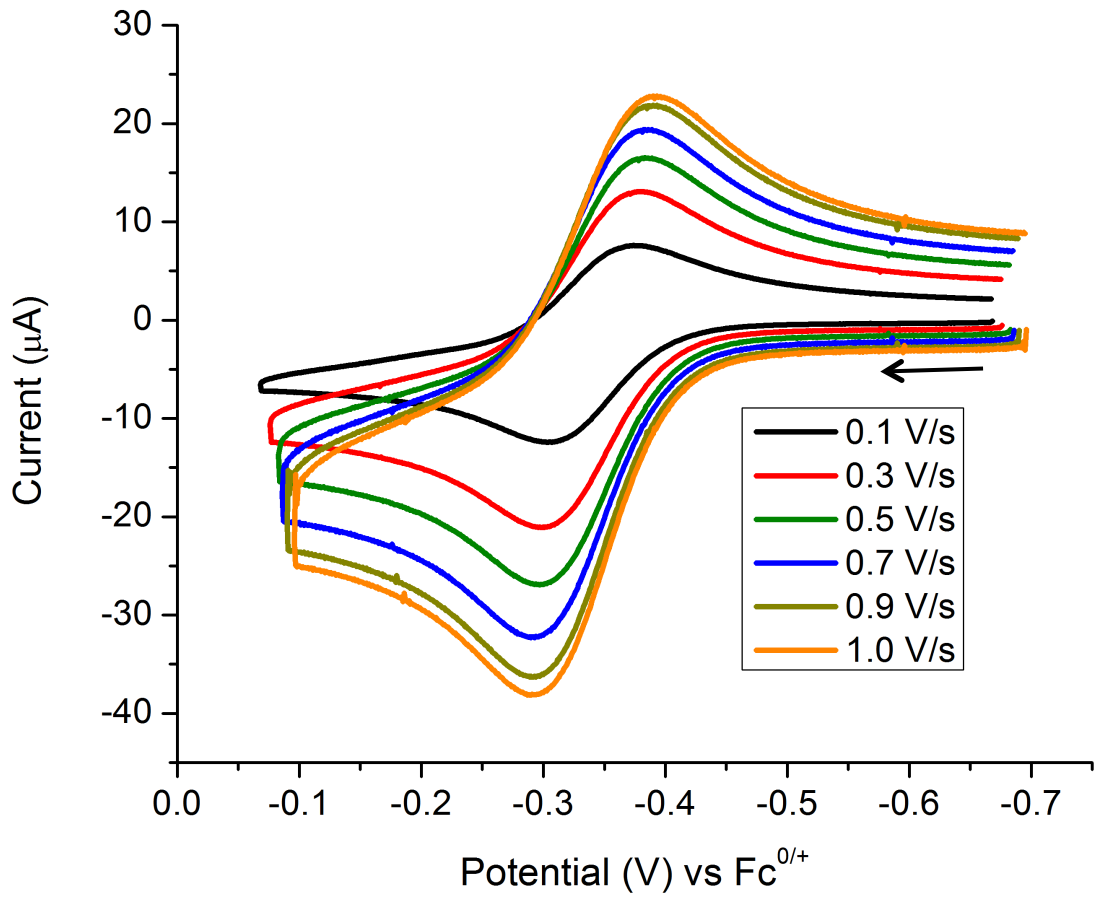

Figure S23. Oxidation of $(Et_4N)_2$[**1**$(BAr^{F\#}{}_3)_2$] in CH_2Cl_2 by Cyclic Voltamogramm.

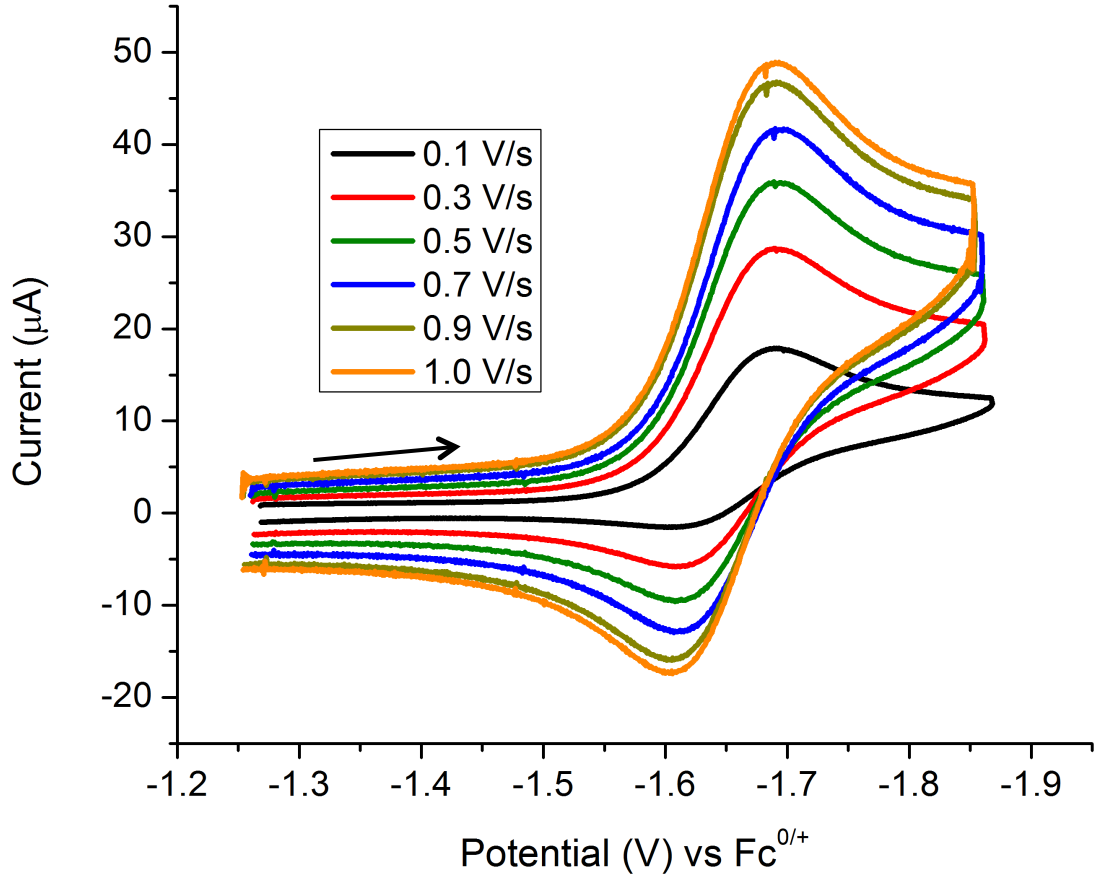

Figure S24. Reduction of $Et_4N[H\mathbf{1}(BAr^F{}_3)_2]$ in CH_2Cl_2 by Cyclic Voltamogramm.

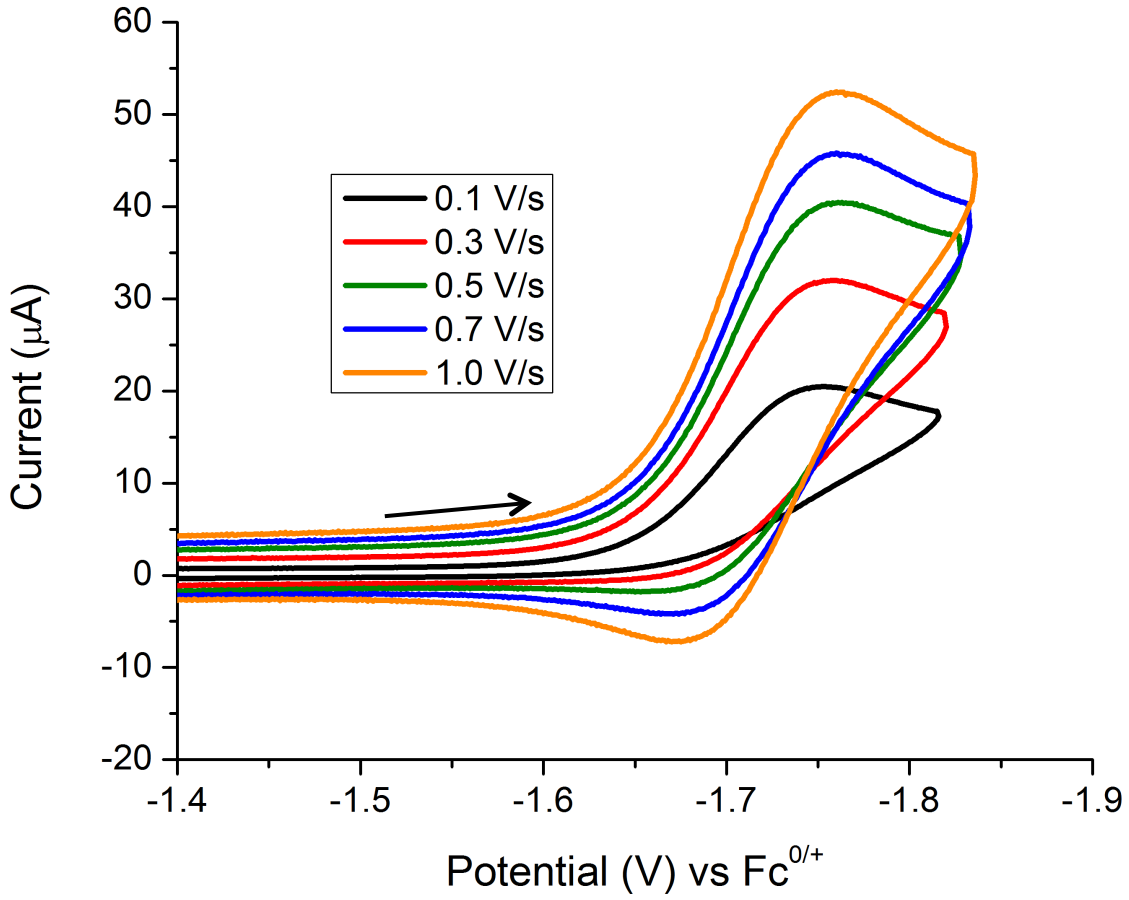

Figure S25. Reduction of $Et_4N[H\mathbf{1}(BPh_3)_2]$ in CH_2Cl_2 by Cyclic Voltamogramm.

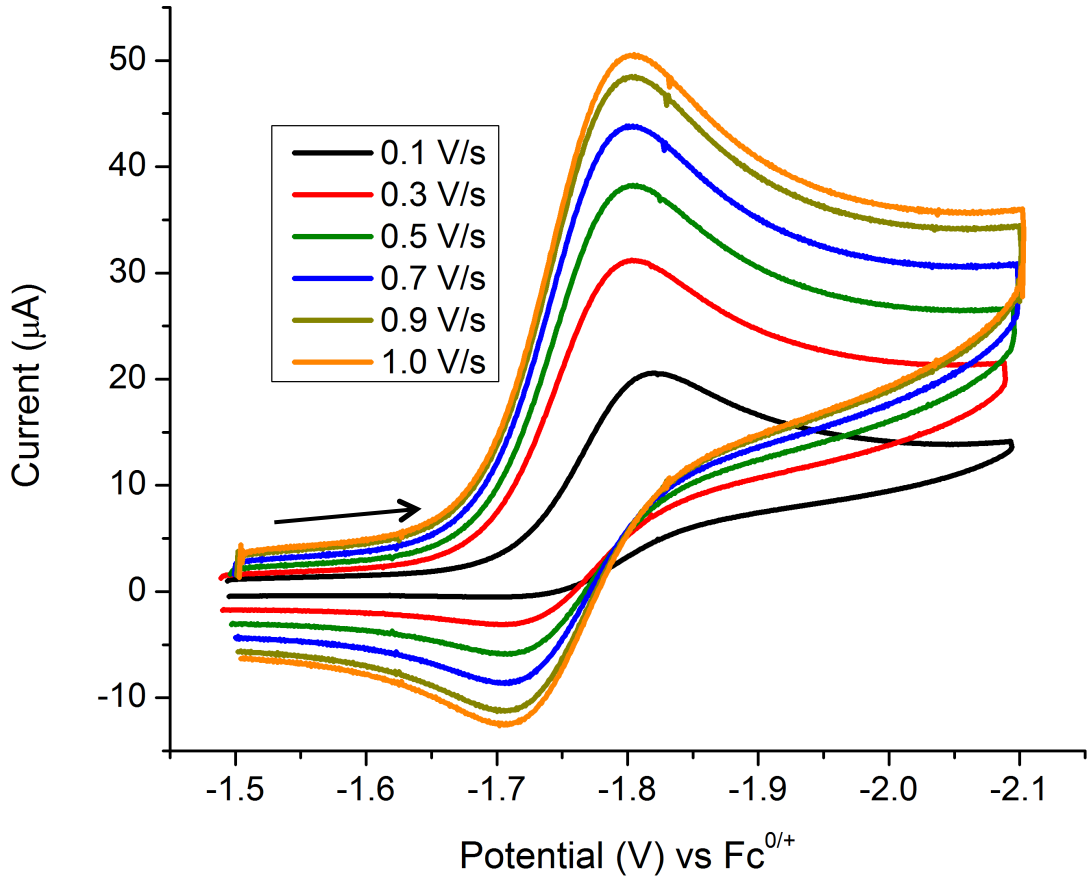

Figure S26. Reduction of $Et_4N[H\mathbf{1}(BAr^{F\#}{}_3)_2]$ in CH_2Cl_2 by Cyclic Voltamogramm.

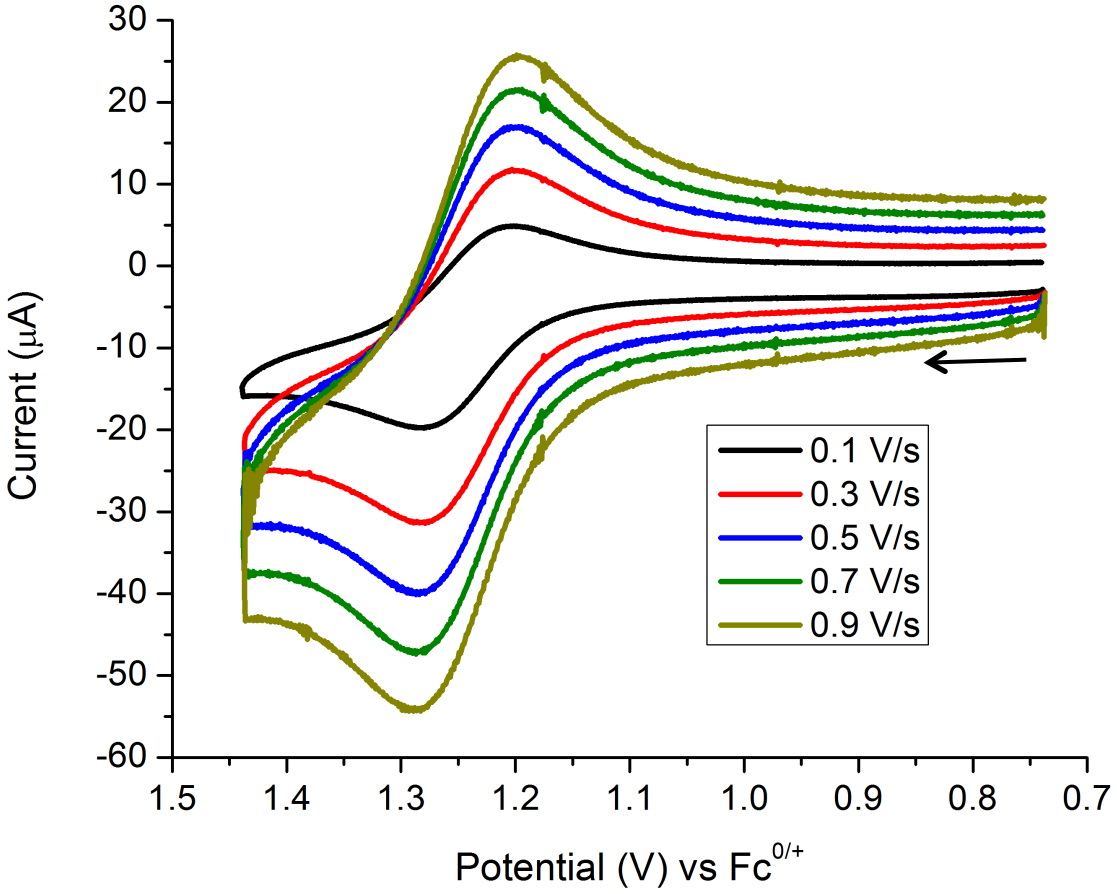

Figure S27. Oxidation of $Et_4N[H\mathbf{1}(BAr^F{}_3)_2]$ in CH_2Cl_2 by Cyclic Voltamogramm.

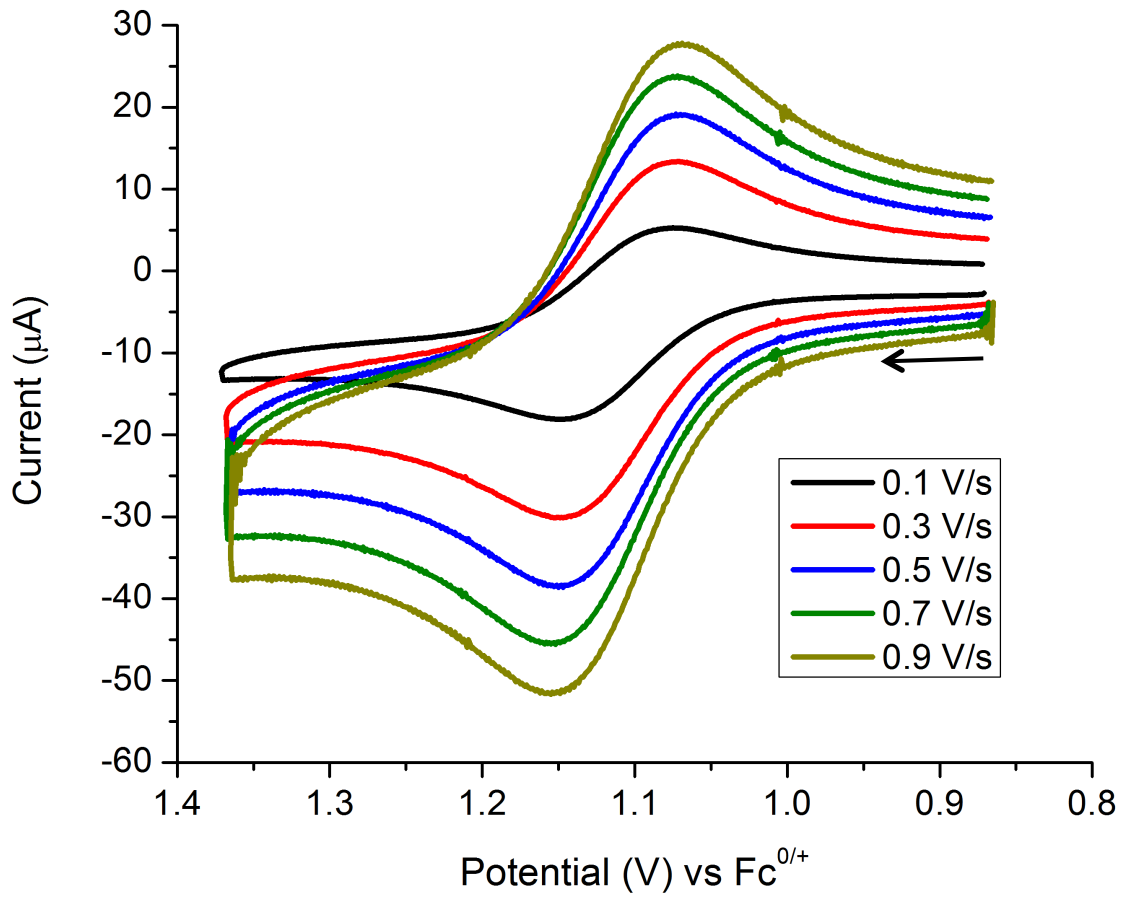

Figure S28. Oxidation of $Et_4N[H\mathbf{1}(BAr^{F\#}{}_3)_2]$ in CH_2Cl_2 by Cyclic Voltamogramm.

References

(1) Schmidt, M.; Contakes, S. M.; Rauchfuss, T. B. *J. Amer. Chem. Soc.* **1999**, *121*, 9736.